

Theoretical investigation of the behavior of reinforced concrete ledge beams

Ahmed S. Alsharkawy

- This paper presents a theoretical investigation of the behavior of reinforced concrete ledge beams that used finite element theory to model the nonlinear behavior of reinforced concrete at all loading stages.
- The three main parameters were the effective thickness of the outer part of the web near the concentrated load where vertical hangers can effectively be placed, the contribution of diagonal bars to the hanging capacity of ledge beams, and the effect of the load eccentricity on the hanging capacity of ledge beams.
- The punching shear behavior of ledge beams was also analyzed using a plasticity-based nonlinear finite element model.

Inverted tee and L ledge beams are widely used in bridge design. They can support bridge girders at a lower elevation than compression-chord-loaded beams can while maintaining a suitable clearance beneath the bridge. In addition, they are used in bridges crossing wide roads or water channels (**Fig. 1**). Ledge beams are also used in precast concrete structures to support precast concrete double-tee beams. In these beams, the ledge is located at the bottom chord where the eccentric concentrated loads are applied and need to be transferred to the compression chord, which in turn produces a tension stress field in the web of these beams.¹⁻³

There are several modes of failure for ledge beams. Ledge beams may fail globally due to global flexure, shear, or torsion. Ledge beams may also fail due to the following local effects (**Fig. 2**):^{4,5}

- yielding of tension tie reinforcement
- crushing of the compression strut under the concentrated load
- separation between the web and the ledge due to hanger reinforcement yielding
- punching shear failure under the concentrated load
- shear friction failure at the shear plane between the ledge and the web
- bearing failure under the supporting plate

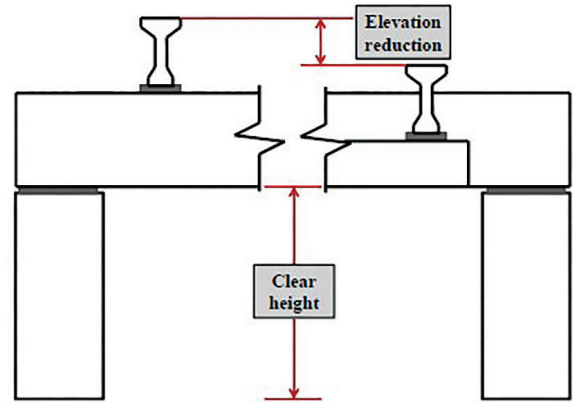


Figure 1. A ledge in a bridge in Alkhalfawy-Shoubra, Egypt. Diagram reproduced with permission from Fernandez-Gomez (2012).

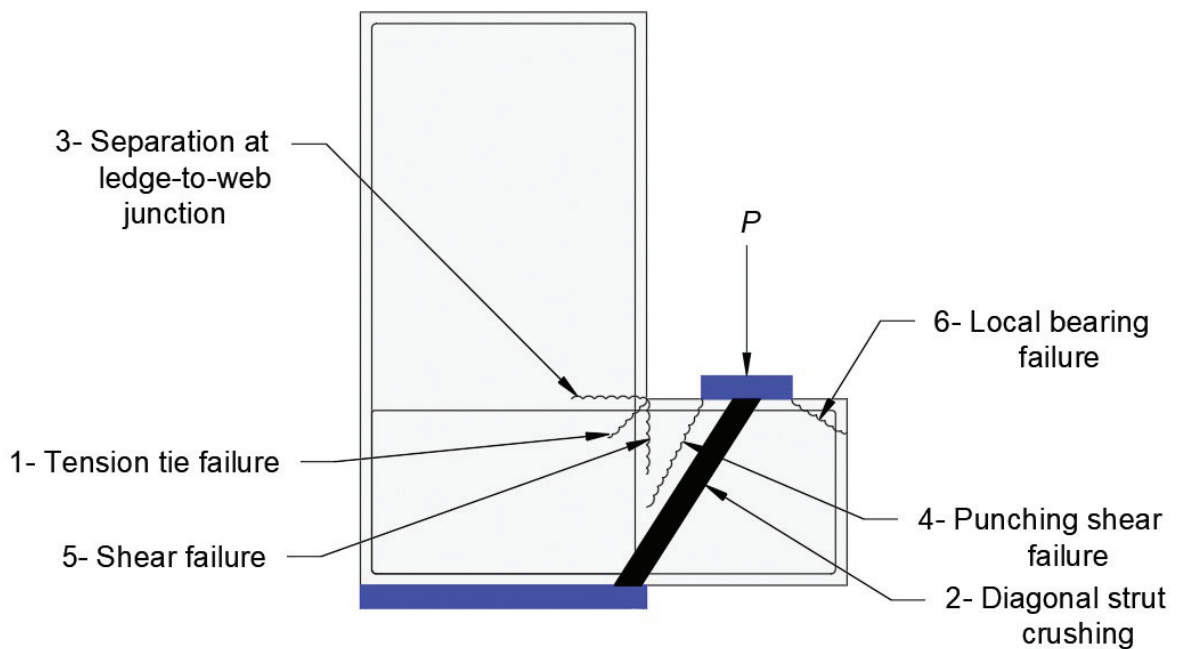


Figure 2. Modes of failure of ledge beams. Note: P = vertical concentrated load.

Design methods to avoid most of these modes of failure of ledge beams are well covered in the literature and in various codes, specifications, and guidelines. However, there are many differences and contradictions among the provisions

found in various publications for two of these modes: separation between the web and the ledge at the web-to-ledge junction due to hanger reinforcement yielding and punching shear failure in the ledge under the concentrated loads. This

paper is focused on these two modes of failure and the possible solutions for them.

Background

Strut-and-tie modeling of ledge beams

Codes, design guidelines, and specifications include simplified equations to directly design ledge beams for all the previously mentioned modes of failure; some of these equations are theoretical, and others are empirical. Strut-and-tie modeling can also be used to design ledge beams. To properly model ledge beams, a three-dimensional (3-D) strut-and-tie model is required (Fig. 3).¹ As in ledge beams, the forces flow in two directions as the compression-chord-loaded beams in addition to the compressive forces in the inclined struts and the tension forces in the horizontal ties in the ledge under the concentrated loads that flow in the third direction. For simplicity, this 3-D strut-and-tie model can be subdivided into two two-dimensional (2-D) models, provided that the interaction between the two models is considered. The two 2-D models are a longitudinal model that consists of an upper strut, bottom tie, vertical ties, and diagonal struts and a cross-sectional model that consists of two horizontal ties, two vertical ties, and two inclined struts.

Comparison of selected design provisions

The provisions related to the design of hanger reinforcement of ledge beams and the estimation of punching shear capacity

of ledges in the Egyptian Code of Practice for Planning, Design, and Construction of Bridges and Elevated Intersections (ECP 207-2015),⁶ the American Association of State Highway and Transportation Officials' *AASHTO LRFD Bridge Design Specifications, 9th edition*,⁴ and the *PCI Design Handbook: Precast and Prestressed Concrete, eighth edition*,⁷ are not identical. To illustrate the differences and similarities in these three publications, relevant provisions from each were applied to example 5.6.1 from the *PCI Design Handbook*. **Table 1** presents the results for the required hanger reinforcement and the punching shear capacity. The results show that there are differences among the calculated total transverse reinforcement areas required by those three references. The total transverse reinforcement area calculated according to the AASHTO LRFD specifications is the largest among the three publications, which can be attributed to the presence of a serviceability check in the AASHTO LRFD specifications. But this check does not exist in the other two references. Concerning punching shear capacity, the results show that there are differences among the calculated demand/capacity ratios according to the three documents. From this example, there are differences and contradictions among the results of the three documents. Therefore, there is a need to investigate the conservativeness and accuracy of the equations proposed in these three documents to estimate the hanging capacity of ledge beams and the punching shear capacity of ledges.

Objectives and scope

Motivated by the differences and the contradictions among the selected design documents, there were two main objectives

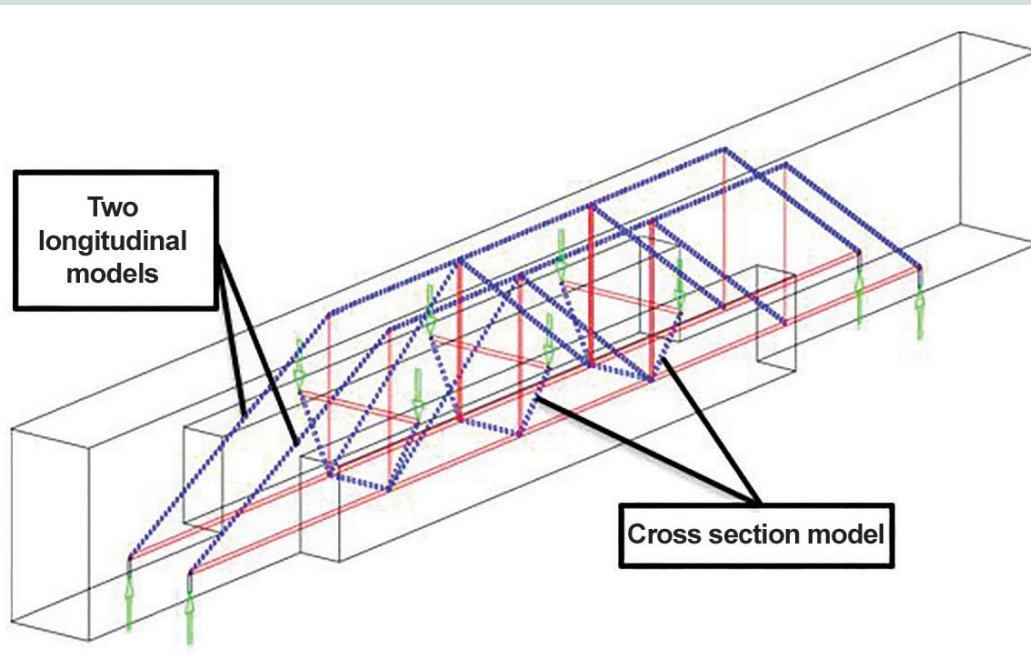


Figure 3. Three-dimensional strut-and-tie model of a ledge beam. Source: Adapted with permission from Fernandez-Gomez (2012).

Table 1. Results of the solved example

Document	ECP 207-2015	PCI 8 th Edition Handbook	AASHTO LRFD 2017	
			Strength	Serviceability
Hanger RFT area, mm ² /m	208	467	193	678
Distribution width, mm	1524	1524	1524	552
Total transverse reinforcement (exterior load, one leg) mm ² /m	682	467	802	1287
Total transverse reinforcement (interior load, one leg) mm ² /m	366	467	459	944
Punching capacity, interior, kN	356.93	250.43	398.92	
<i>D/C</i> , interior	1.28	1.1	1.75	
Punching capacity, end, kN	510.08	239.31	398.92	
<i>D/C</i> , end	0.9	1.83	1.1	

Note: C = capacity; D = demand. 1 mm = 0.0394 in.; 1 m = 3.281 ft; 1 kN = 0.225 kip.

for the study reported in this paper. The first objective was to investigate the effective thickness of the outer part of the web near the concentrated load where vertical hangers can effectively be placed (inner stirrup leg distance from the outer face of the web X_i), the contribution of diagonal bars to the hanging capacity of ledge beams, and the effect of load eccentricity on the hanging capacity of ledge beams. The second objective was to investigate the capability of a plasticity-based nonlinear finite element model to estimate punching shear failure in ledges. In addition, the accuracy and the conservativeness of the equations from the ECP 207-2015, AASHTO LRFD specifications, and *PCI Design Handbook* that are used to estimate the hanging capacity of ledge beams and the punching shear capacity of ledges were evaluated.

In this paper, the basic assumptions adopted in analysis of the studied ledge beams are described, including cross-sectional dimensions, reinforcement, and material properties, present details of the development of a comprehensive finite element model (FEM) to perform nonlinear analysis for reinforced concrete ledge beams and validate the developed FEM by modeling three reinforced concrete ledge beams that were experimentally tested in the literature. The hanging capacities estimated by the plasticity-based nonlinear FEM are then used to investigate the effects of using inner stirrup legs or diagonal bars and the effect of the load eccentricity on hanging capacity of ledge beams. Finally, the punching shear capacities estimated by the plasticity-based nonlinear FEM are compared with experimental results collected from the literature to investigate the accuracy of the results. The estimated results from the FEM are used as a reference for the hanging capacity investigations because there is a lack of experimental data. Experimental data are used as a reference for the punching shear investigations.

Basic assumptions

In this study, nonlinear finite element software was used to analyze 18 theoretical reinforced concrete ledge beams. All these beams are L-shaped ledge beams with a clear span of

13 m (43 ft). The beams support four girders spaced at 3.5 m (11 ft), and the reaction of each girder is transferred to the ledge through a bearing pad with a width of 0.5 m (1.6 ft). The beams are hinged-roller, simply supported elements with two supporting plates 0.5 m in width, and they are supported laterally with four anchors to restrain the rotation of the beams. The beams are designed according to ECP-207-2015, taking into consideration that the failure due to yielding of hanger reinforcement happens before the failure due to punching shear in the ledge to make sure that the failure is ductile. **Figure 4** presents an elevation and cross sections for the beams.

These 18 beams include the following:

- Seven beams—H1, H2, H3, H4, H5, H6, and H7—with inner stirrup legs at distances X_i of 60, 120, 180, 240, 300, 360, and 400 mm (2.4, 4.7, 7.1, 9.4, 12, 14, and 16 in.), respectively, from the outer face of the web. Those seven beams were analyzed to investigate the contribution of the inner stirrup legs to the hanging capacity of ledge beams, and the results were compared to control beam H0 without inner stirrup legs. The seven beams had a load eccentricity e of 350 mm (14 in.) from the web of the beams.
- Six beams—E1, E2, E3, E4, E5, and E6—with load eccentricities e of 100, 200, 300, 400, 500, and 600 mm (4, 8, 12, 16, 20, and 24 in.), respectively, from the web. These beams were analyzed to investigate the effect of load eccentricity on the hanging capacity of ledge beams, and the results were compared to control beam E0 with a load eccentricity e of 350 mm (14 in.) from the web.
- Beams D_1 and D_2 . D_1 has inner stirrup legs at a distance X_i of 60 mm (2.4 in.) from the outer face of the web, and D_2 has diagonal bars. These two beams were analyzed to investigate the contribution of diagonal bars to the hanging capacity of ledge beams, and the results were compared with results for control beam D_0 without inner stirrup legs or diagonal bars.

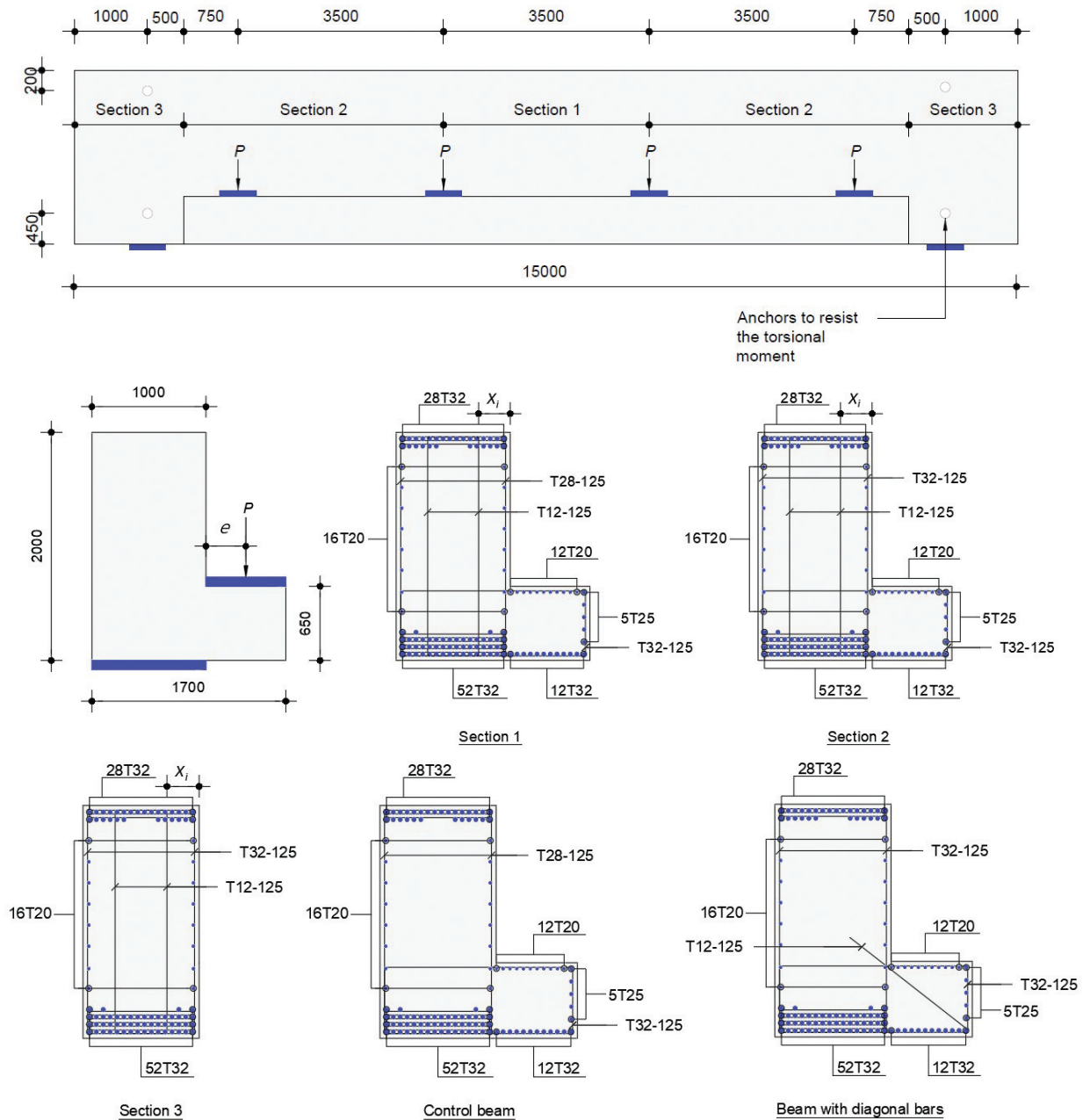


Figure 4. Geometry and design details for the ledge beams. Note: e = load eccentricity; P = concentrated vertical load; X_i = inner stirrup leg distance from the outer face of the web. All measurements are in millimeters. 1 mm = 0.0394 in.

The material properties of the concrete are assumed to be as follows: compressive strength f'_c of 32 MPa (4600 psi), Poisson's ratio ν_c of 0.2, and modulus of elasticity E_c of 27,828 MPa (4036.0 ksi).

The material properties of the steel are assumed to be as follows: yield stress f_y of 400 MPa (58 ksi), ultimate stress f_u of 600 MPa (87 ksi), Poisson's ratio ν_s of 0.3, and modulus of elasticity E_s of 200,000 MPa (29,000 ksi).

The punching shear capacities estimated by the plastici-

ty-based nonlinear FEM were compared with the punching shear capacities of four short-span ledge beams (RS3-D, RS4, RS5-D, and RS7) and six long-span ledge beams (LB1, LB2, LB3, LB3-RQ, LB3-LQ, LB4, and LB6) that were experimentally tested by Nafadi.⁸ Nafadi et al.⁹⁻¹¹ has details about the geometry, reinforcement, loading mechanism, and materials properties of the beams.

Finite element simulations

Methodology

In this study, concrete was modeled using an eight-noded hexahedral linear brick with reduced integration (one integration point) and hourglass control. These elements are suitable for 3-D materials. Also, this type of element is typically used when plasticity and large deformations are expected, such as in the case of concrete structures. The linear reduced-integration option was used throughout the analysis of concrete parts in this study. This option is capable of withstanding severe distortions, and it reduces the time required for the analysis. However, this option also could affect the analysis results; therefore, it is important to pay attention to this possibility when comparing the analytical results with experimental results. The concrete damaged plasticity model was chosen to numerically model the behavior of concrete in this study.

Reinforcement was modeled using a 3-D, two-node truss element. This element is used to model slender elements that only support axial forces without any moments. A material property and a cross-sectional area can also be assigned to this element.

Concrete damaged plasticity model

The concrete damaged plasticity model developed by Lubliner et al.¹² is a modification of the Drucker-Prager strength hypothesis.¹³ The failure surface of triaxially loaded concrete is a 3-D surface. According to Drucker-Prager strength hypothesis, the failure surface is assumed to take a 3-D cone shape with

a circular deviatoric cross section (Fig. 5). Any point inside this surface is considered as a safe behavior. The yield surface and the plastic potential surface are also inside this surface. This assumption offers a smooth boundary surface without any computational problems, but this behavior is not compatible with the real concrete behavior. Given this drawback in Drucker-Prager strength hypothesis, Lubliner et al. modified the hypothesis and developed the concrete damaged plasticity model. The yield surface in the concrete damaged plasticity model can be developed according to Eq. (1).

$$F = \frac{1}{1-\alpha} \left[\bar{q} - 3\alpha\bar{p} + \beta \left(\varepsilon_t^{pl}, \varepsilon_c^{pl} \right) \langle \bar{\sigma}_{max} \rangle - \gamma \langle -\bar{\sigma}_{max} \rangle \right] - \bar{\sigma}_c \varepsilon_c^{pl} \quad (1)$$

where

F = yield function

\bar{p} = effective hydrostatic pressure

\bar{q} = equivalent von Mises stress

α = dimensionless material constant (defined in Eq. [2])

β = dimensionless material constant (defined in Eq. [3])

γ = dimensionless material constant (defined in Eq. ([4])

ε_c^{pl} = the plastic compressive strain

ε_t^{pl} = the plastic tensile strain

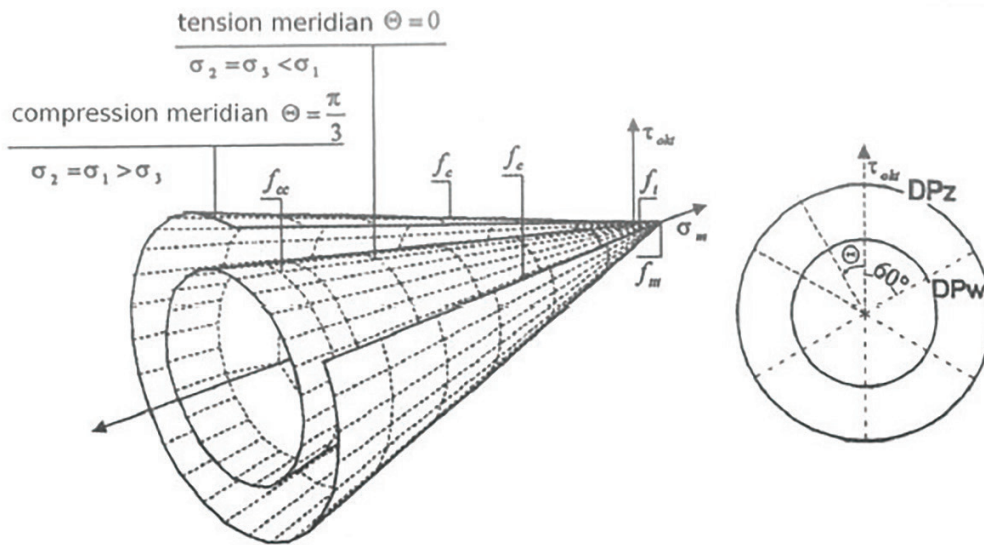


Figure 5. Drucker-Prager boundary surface. Source: Reproduced with permission from Kmiecik and Kamiński (2011). Note: D = abbreviation for deviatoric plan; f_c = uniaxial compressive stress; f_{cc} = biaxial compressive stress; f_m = the mean stress; f_t = tensile stress; P_w = yield surface in the deviatoric plan; P_z = failure surface in the deviatoric plan; Θ = lode angle; σ_1 = major principal effective stress; σ_2 = intermediate principal effective stress; σ_3 = minor principal effective stress; σ_m = the hydrostatic stress; τ_{oct} = octahedral shear stress.

$\bar{\sigma}_c$ = the effective compressive stress
 $\bar{\sigma}_{max}$ = algebraically maximum eigenvalues of tensor

Macauley bracket function $\langle X \rangle = \frac{1}{2} \langle X + |X| \rangle$

$$\alpha = \frac{\left(\frac{\sigma_{bo}}{\sigma_{co}} \right) - 1}{2 \left(\frac{\sigma_{bo}}{\sigma_{co}} \right) - 1} \quad 0 \leq \alpha \leq 0.5 \quad (2)$$

where

σ_{bo} = biaxial compressive stress
 σ_{co} = uniaxial compressive strength
 $\frac{\sigma_{bo}}{\sigma_{co}} = 1.16$

$$\beta = \frac{\bar{\sigma}_c \varepsilon_c^{pl}}{\bar{\sigma}_t \varepsilon_t^{pl}} (1 - \alpha) - (1 + \alpha) \quad (3)$$

where

$\bar{\sigma}_c$ = effective cohesive stresses for compression
 $\bar{\sigma}_t$ = effective cohesive stresses for tension

$$\gamma = \frac{3(1 - K_c)}{2K_c - 1} \quad (4)$$

where

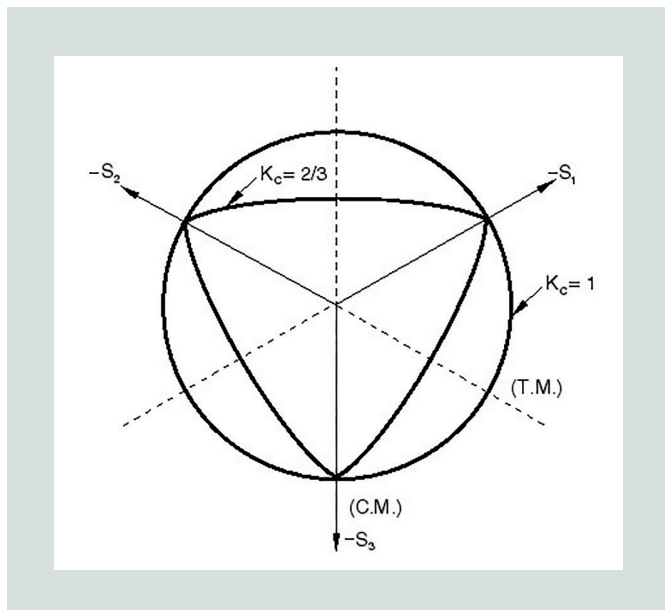


Figure 6. Yield surfaces in the deviatoric plane, corresponding to different values of K_c . Note: K_c = ratio between the distances of the tension meridian and the compression meridian on the hydrostatic axis; S_1 = major principal effective stress; S_2 = intermediate principal effective stress; S_3 = minor principal effective stress.

K_c = ratio between the distances of the tension meridian and the compression meridian on the hydrostatic axis

The coefficient γ appears only for the triaxial compression stress state and can be determined by comparing the yield conditions along the tensile and compressive meridians. The variable K_c should be estimated based on a full triaxial test. The value of K_c ranges from 0.5 to 1. The nonlinear finite element software recommends a value of $\frac{2}{3}$ as a default value for K_c . If K_c equals 1, the shape of the yield surface in the deviatoric cross section will be a circle, as in Drucker-Prager hypothesis¹³ (Fig. 6).

The flow rule is used to connect the yield surface stress and the concrete stress-strain relationship. The concrete damaged plasticity model used Drucker-Prager hyperbolic function as a nonassociated flow potential function according to Eq. (5).

$$G = \sqrt{(\varepsilon \sigma_{io} \tan \phi)^2 + \bar{q}^2} - \bar{p} \tan \phi \quad (5)$$

where

G = flow potential function
 ε = eccentricity that is a positive value expressing the rate of approach of the plastic potential hyperbola to its asymptote
 σ_{io} = the uniaxial tensile strength
 ϕ = dilation angle that physically represents the internal friction angle of concrete

The nonlinear finite element software gives a value of 0.1 as a default value for ε , which means that the dilation angle of the concrete is constant along a wide range of confining pressure. The dilation angle ϕ represents the angle of inclination of the yield surface in the meridional plane. The value of the dilation angle of concrete ranges from 30 to 42 degrees. In this study, a sensitivity analysis was performed and a value of 34 degrees for this angle was chosen.

Damage is also introduced in the model through the damage parameter d according to Eq. (6).

$$\sigma = (1 - d) \bar{\sigma} = \frac{E_o}{(\varepsilon - \varepsilon^{pl})} \quad (6)$$

where

σ = uniaxial compressive stress
 $\bar{\sigma}$ = effective compressive stress
 E_o = initial undamaged elastic modulus of concrete
 ε = total strain

ε_{pl} = plastic strain of concrete

Material models

Concrete uniaxial compression model The literature provides several models to describe the behavior of concrete under uniaxial compression, and three of them were considered for this study: the Eurocode model,¹⁴ the Hognestad model,¹⁵ and the Carreira and Chu model.¹⁶ Based on a sensitivity study, the Hognestad model was chosen for this study. The Hognestad model for uniaxial compression behavior of concrete consists of three stages (Fig. 7). The first stage represents the linear elastic behavior of concrete with an initial modulus of elasticity E_o equal to $5500\sqrt{f'_c}$, and this stage continues to a uniaxial compressive stress σ_{co} equal to $0.4f'_c$, which is the same level stated in the Eurocode model. This stage is followed by the second stage, which represents the ascending branch and continues until the maximum stress of concrete f'_c , which corresponds to a strain ε_o corresponding to the peak stress and equal to $2f'_c/E_{sec}$ with a secant modulus of elasticity E_{sec} equal to $5000\sqrt{f'_c}$. Finally, there is the third stage, which represents the descending or the post-peak branch from the peak stress f'_c to the ultimate strain ε_u , which equals 0.0038. Eq. (7) gives the relation between the concrete stress σ_c and strain ε_c for the Hognestad model.

$$\sigma_c = f'_c \left[2 \left(\frac{\varepsilon_c}{\varepsilon_o} \right) - \left(\frac{\varepsilon_c}{\varepsilon_o} \right)^2 \right] \quad (7)$$

Concrete uniaxial tension model The literature has several models to describe the behavior of concrete under uniaxial tension, and three of them were considered for this study:

- the modified Nayal and Rasheed model¹⁷

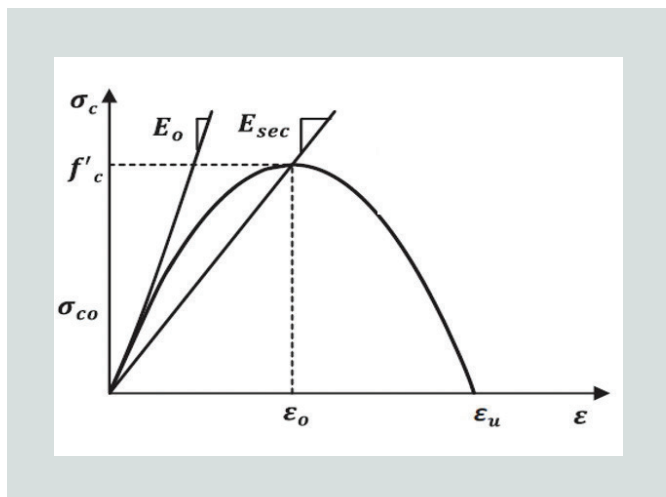


Figure 7. Hognestad model for uniaxial compression behavior of concrete. Source: Reproduced with permission from Genikomsou and Polak (2015). Note: E_o = initial undamaged elastic modulus of concrete; E_{sec} = secant modulus of elasticity; f'_c = compressive strength of concrete; ε = total strain; ε_o = the strain corresponding to the max compressive stress; ε_u = ultimate strain; σ_{co} = uniaxial compressive strength; σ_c = concrete stress.

- the modified Wang and Hsu model¹⁸
- the Carreira and Chu model¹⁹

Based on a sensitivity study, the modified Wang and Hsu model was chosen for this study. That model takes into consideration interlocking aggregates; the adhesive force between the reinforcement and the concrete; the stress transferred from the reinforcement to the uncracked concrete, which makes the concrete between cracks contribute to the tensile strength; and the dowel action. Therefore, the proposed weakening branch is a curve not a line. The proposed model is defined by Eq. (8) for the linear part until the maximum tensile stress and by Eq. (9), which represents the weakening function.

$$\sigma_t = E_t \varepsilon_t \quad \text{if } \varepsilon_t \leq \varepsilon_{cr} \quad (8)$$

where

σ_t = tension stress

E_t = modulus of elasticity of concrete in tension

ε_t = tension strain

ε_{cr} = cracking strain

$$\sigma_t = f_t \left(\frac{\varepsilon_{cr}}{\varepsilon_t} \right)^n \quad \text{if } \varepsilon_t > \varepsilon_{cr} \quad (9)$$

where

f_t = tensile stress

n = rate of weakening = 0.5 based on a sensitivity study

Reinforcement model There are two hypotheses for modeling reinforcement behavior in tension.²⁰ The first considers reinforcement as an elastic-perfectly plastic material. In this model, the reinforcement behaves as an elastic material until the yield point is reached, and then it behaves as a perfectly plastic material without strain hardening (Fig. 8). The second model is the backbone model (Fig. 9). This model represents the tension behavior of reinforcement through four stages. The first stage is the linear elastic stage, which ends at the yielding point. The second stage is a yielding plateau, which continues until the strain hardening point. The third stage starts at the strain hardening point and continues to the ultimate point. The final stage represents the post-ultimate-plateau phase; it starts from the ultimate point and continues until failure. The elastic/perfectly plastic model was selected for this study based on a sensitivity study.

Interaction between model elements

The interaction between reinforcement and concrete is modeled using the embedded constraint. The concrete acts as a host

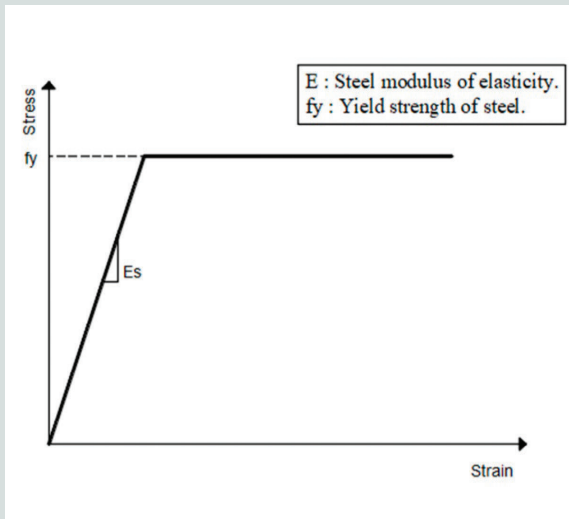


Figure 8. Elastic/perfectly plastic model for tension behavior of reinforcement. Note: E_s = modulus of elasticity of steel; f_y = yield stress of steel.

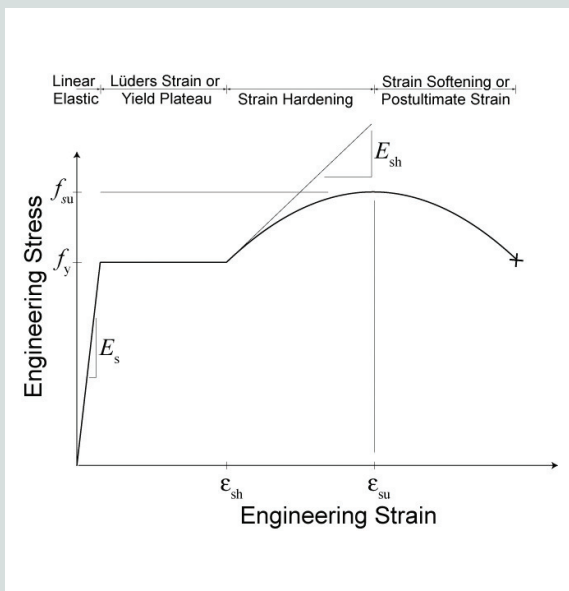


Figure 9. Backbone model for tension behavior of reinforcement. Note: E_s = modulus of elasticity of steel; E_{sh} = modulus of plasticity of steel reinforcing bars in strain hardening stage; f_{su} = max stress; f_y = yield stress of steel; ϵ_{sh} = strain in steel reinforcement in strain hardening stage; ϵ_{su} = strain in steel reinforcement corresponding to the peak stress.

region, and the reinforcement acts as an embedded region. This means that the nodes of the reinforcement do completely obey the translations and the rotations of the concrete element nodes, thereby, representing a perfect bond between them without any slippage. But this manner isn't accurate. However, the concrete damaged plasticity model can capture the damage between the reinforcement and the concrete. The interaction between the concrete and any loading or support plate is modeled using

the tie constraint, the plates act as master surfaces, and the concrete acts as a slave surface. The interaction between the concrete and any reference point is modeled using the coupling constraint, the concrete acts as the constraint surface, and the reference point acts as the control point.

Finite element model validation

Experimental data for three ledge beams—SL3-42-1.85-06, A1, and SS1-75-1.85-03—were collected from the literature. Fernandez-Gomez¹ provides details of the geometry and reinforcement of SL3-42-1.85-06 and SS1-75-1.85-03. El Badawy²¹ provides information on beam A1. The beams were modeled using nonlinear finite element software, with the materials models and parameters discussed previously. The analytical and experimental results were then compared to ensure that the proposed materials models were capable of accurately capturing the behavior of ledge beams as a first step toward using these models in this study. **Figures 10, 11, and 12** compare the analytical and experimental results in terms of a load-deflection relationship. The results indicate good correlation between the experimental and the analytical results. The analytical results showed stiffer behavior than the experimental results. Initial cracking due to shrinkage and the accuracy of the representation of tension stiffening could be reasons for the deviation.

Investigation of hanging action of ledge beams

The 18 theoretical reinforced concrete ledge beams were analyzed using nonlinear finite element software (**Fig. 13**). The failure criterion that was used in the analysis is designed to take into consideration the integration and stability of the beam until the failure. Hanger reinforcement can yield and reach a yielding plateau without fracture, but the crack width between the web and the ledge increases excessively, which in

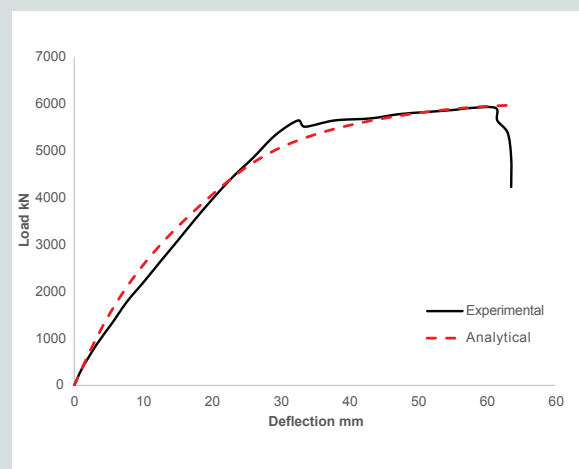


Figure 10. Load deflection curves for beam SL3-42-1.85-06. Note: 1 mm = 0.0394 in.; 1 kN = 0.225 kip.

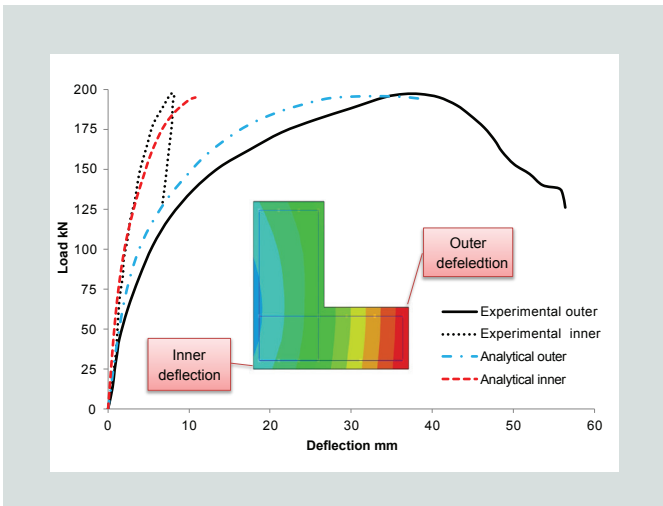


Figure 11. Load deflection curves for beam A1. Note: 1 mm = 0.0394 in.; 1 kN = 0.225 kip.

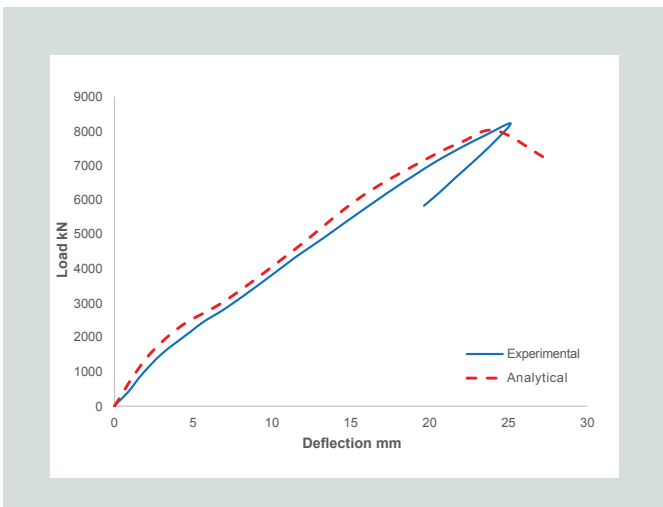


Figure 12. Load deflection curves for beam SS1-75-1.85-03. Note: 1 mm = 0.0394 in.; 1 kN = 0.225 kip.

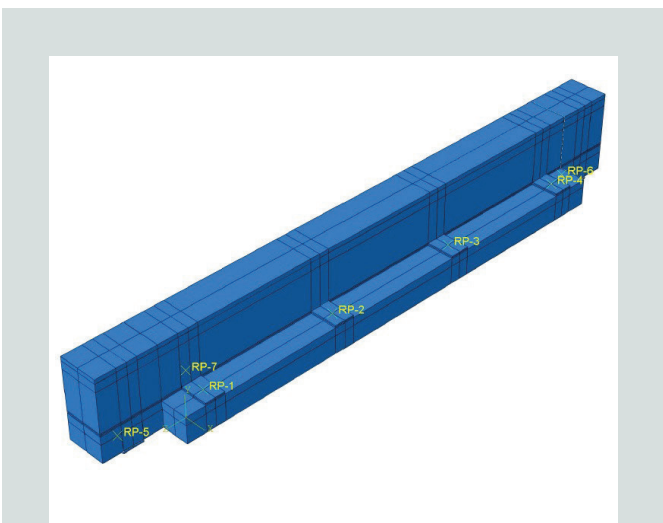


Figure 13. Nonlinear finite element software model of a ledge beam.

turn affects the integration and stability of the beam and may lead to corrosion of the reinforcement. Therefore, to ensure that the beam would remain stable and integrated, the stress in the hanger reinforcement was checked to be less than the fracture strength, and the crack width at the web-to-ledge junction was checked to be within a limited value. The crack width at the web-to-ledge junction can be calculated using the strains in the hanger reinforcement H and the ledge flexural reinforcement F according to Eq. (10) and (11) for interior and exterior loads, respectively.²²

$$W = L_{HF} \epsilon_{HF} \leq 0.812 \text{ mm} \quad (10)$$

where

W = crack width at the web-to-ledge junction

L_{HF} = compatibility-aided strut-and-tie model gauge length = $(9500\epsilon_{HF} - 3 \text{ in.})$

ϵ_{HF} = diagonal crack strain = $\sqrt{\epsilon_H^2 + \epsilon_F^2}$ (Fig. 14)

ϵ_H = strain in the hanger reinforcement

ϵ_F = strain in the ledge flexural reinforcement

$$W = \frac{2.6L_{HF}\epsilon_{HF}}{(1+0.7L_E)} \leq 0.203 \quad (11)$$

where

L_E = distance from the beam end and the center of the first exterior load

The allowable values for the crack width at the web-to-ledge junction are 0.812 and 0.203 mm (0.0320 and 0.00799 in.) for the interior and the exterior loads, respectively. These values are selected according to the American Concrete Institute's

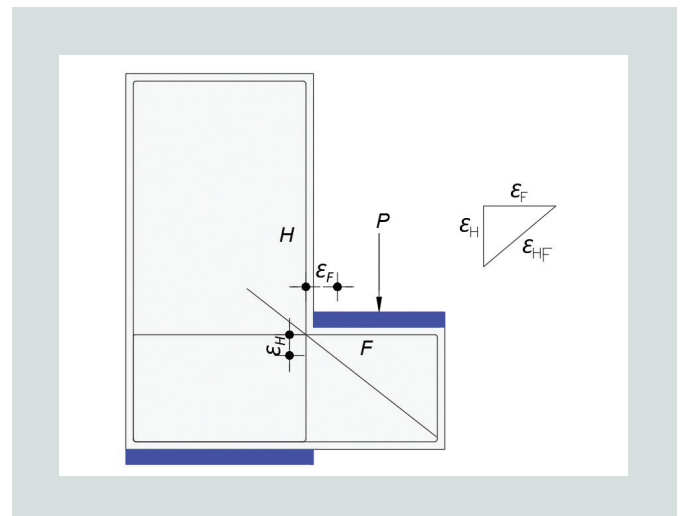


Figure 14. Crack strains. Note: F = ledge flexural reinforcement; H = hanger reinforcement; P = axial load; ϵ_F = strain in the ledge flexural reinforcement; ϵ_H = strain in the hanger reinforcement; ϵ_{HF} = diagonal crack strain.

Control of Cracking in Concrete Structures (ACI PRC- 224R-01)²³ after incorporating the scaling ratio S . The scaling ratio S accounts for the change in size between the tested beam and the beam under consideration, which will affect the gauge length. It is calculated according to Eq. (12)²² and equals 1.98 for the ledge beams used in this study.

$$S = \left[\frac{(d_e - c - 0.5d_b)_p (a_f)_p (A_{SH})_p}{(d_e - c - 0.5d_b)_T (a_f)_T (A_{SH})_T} \right]^{1/4} \quad (12)$$

where

- d_e = effective depth of the ledge, which is taken as the distance from the bottom of the ledge to the center of the top flexural reinforcing bars in the ledge
- c = concrete cover
- d_b = diameter of the bottom reinforcing bars in the ledge
- a_f = distance from the load center line to the hanger reinforcement
- A_{SH} = area of one of the reinforcing bar used as hanger reinforcement
- p = proposed beam under consideration
- T = tested beam

Punching shear of ledges

Nonlinear finite element software was used to analyze the 10 ledge beams that were experimentally tested by Nafadi⁸ (Fig. 15). The failure criteria used for these 10 beams consid-

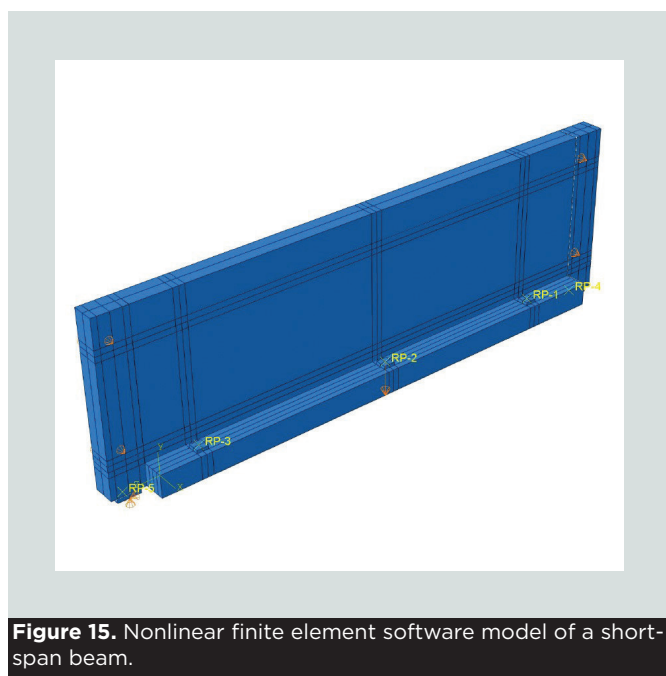


Figure 15. Nonlinear finite element software model of a short-span beam.

er the punching shear failure in ledges under the concentrated loads to take place when the maximum principal compressive strain in the punching cone under this load reaches a value of 0.002 (Fig. 16). These criteria are used by many researchers in the literature.^{8,15,24}

Results

Hanging action

Comparison of code and specifications

Table 2 compares the finite element estimates for the hanging capacities of ledge beams H0 (control), H1, H2, H3, H4, H5, H6, H7, E0 (control), E1, E2, E3, E4, E5, and E6, with the hanging capacity results calculated in accordance with provisions from the ECP 207-2015, the AASHTO LRFD specifications, and the *PCI Design Handbook*. Calculations based on ECP 207-2015 and AASHTO LRFD specifications overestimated the hanging capacities of the investigated ledge beams because the equations neglect the load eccentricity effect on the hanging capacity. In contrast, calculations based on the *PCI Design Handbook* underestimated the hanging capacity of the investigated ledge beams as the equation considers the load eccentricity effect but does not consider the contribution of the inner legs. Based on these findings, it is recommended to use the equation from the *PCI Design Handbook* to design the required hanger reinforcement.

Contribution of inner stirrup legs Figure 17 shows the finite element estimates of the hanging capacity of the beams analyzed to investigate the contribution of the inner legs to the hanging capacity of ledge beams. The results demonstrate that using inner legs as hanger reinforcement increased the hanging capacity of the analyzed beams with varied ratios depending on the location of the inner legs relative to the outer face of the web X_i or depending on X_i/b , where b is the width of the web.

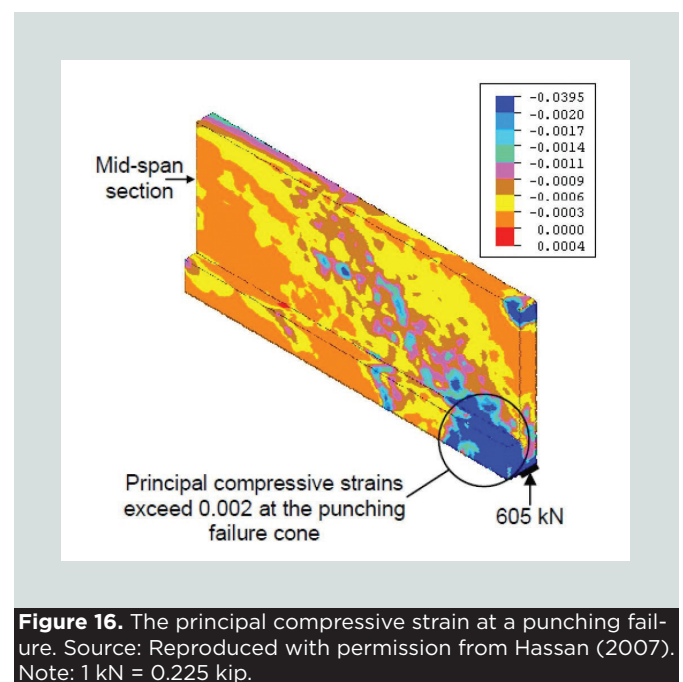


Figure 16. The principal compressive strain at a punching failure. Source: Reproduced with permission from Hassan (2007). Note: 1 kN = 0.225 kip.

Table 2. Comparison among codes

Beam	ECP and AASHTO failure load, kN	PCI failure load, kN	FEM failure load, kN	ECP and AASHTO/FEM	PCI/FEM
H0	1538.248	1296.4	1394.73	1.102	0.929
H1	1538.248	1296.4	1562.09	0.984	0.829
H2	1538.248	1296.4	1543.41	0.996	0.84
H3	1538.248	1296.4	1524.8	1.008	0.85
H4	1538.248	1296.4	1506.24	1.021	0.86
H5	1538.248	1296.4	1487.56	1.034	0.871
H6	1538.248	1296.4	1468.85	1.047	0.882
H7	1538.248	1296.4	1450.16	1.06	0.894
E0	1538.248	1296.4	1394.7	1.102	0.929
E1	1538.248	1661	1532.6	1.003	1.083
E2	1538.248	1493.1	1497.7	1.027	0.996
E3	1538.248	1356	1431.9	1.074	0.947
E4	1538.248	1241.9	1381.1	1.113	0.899
E5	1538.248	1145.6	1299.7	1.183	0.881
E6	1538.248	1063.1	1217.5	1.263	0.873

Note: AASHTO = AASHTO LRFD specifications; ECP = ECP 207-2015; FEM = finite element model; PCI = *PCI Design Manual*. 1 kN = 0.225 kip.

The hanging capacity is increased by 12%, 10.66%, 9.33%, 8%, 6.67%, 5.33%, and 4% for X_i/b of 6%, 12%, 18%, 24%, 30%, 36%, and 42%, respectively. **Figure 18** shows the stress in the inner stirrup legs depending on the X_i/b as a ratio from the yield strength. As the X_i/b increases, the stress in the reinforcement of these legs decreases. It is recommended to arrange the inner legs that are intended to contribute to increasing the hanging capacity of ledge beams at the smallest X_i/b possible to make the best use

of these legs to increase the hanging capacity of these beams. Consequently, it is recommended to consider the maximum X_i/b to be in the range of 30% to 40% but not more than 40%.

Load eccentricity effect **Figure 19** presents the finite element estimates of the hanging capacities of the beams analyzed to investigate the load eccentricity effect on the hanging capacity of ledge beams. The results emphasize that the effect

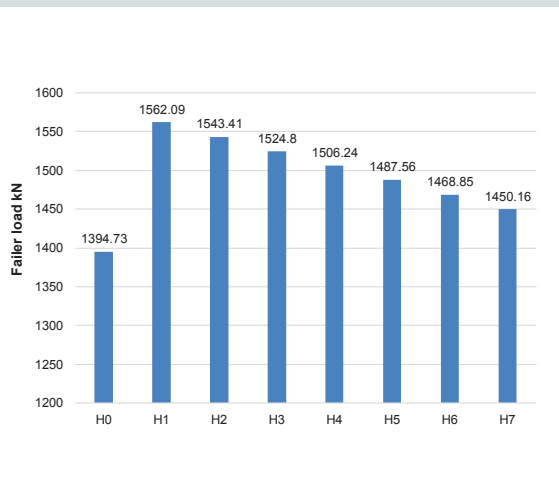


Figure 17. Inner stirrup legs' contribution to the hanging capacity of ledge beams. Note: 1 kN = 0.225 kip.

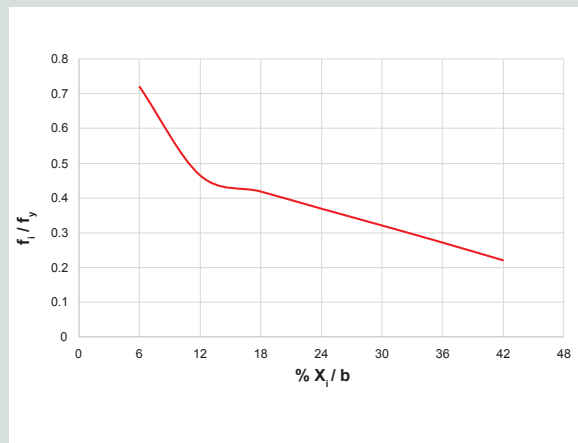


Figure 18. The relationship between the ratio X_i/b and stress in the inner legs. Note: b = the width of the web; f_i = the stress in the inner stirrup branch; f_y = yield stress of steel; X_i = inner stirrup leg distance from the outer face of the web.

of the load eccentricity e is major and cannot be neglected. The hanging capacity of the analyzed beams decreases as the load eccentricity increases. The hanging capacity is reduced by up to 26.344%; therefore, it is recommended that codes and specifications take the load eccentricity effect into consideration in design equations.

Diagonal bars effect Figures 20 and 21 show the finite element estimates of the hanging capacity of the beams analyzed to investigate the effect of diagonal bars on the hanging capacity of ledge beams in terms of the failure load and the cracking load, respectively. The results indicate that in the beams using diagonal bars, the failure load and the cracking load were increased by 7.51% and 18.27%, respectively, compared with the control beam. The failure load and the cracking load were increased 12% and 9.64%, respectively, for the beam with inner legs at 60 mm (2.4 in.) from the outer face of the web. The effect of the diagonal bars on the cracking load is more pronounced.

Figure 22 presents the failure loads for the beam with diagonal bars and the beams with inner legs at different X_i/b . For X_i/b equal to or less than 24%, using inner legs is more effective than using diagonal bars to increase the failure

load. However, for X_i/b greater than 24%, diagonal bars are more effective than inner legs to increase the failure load. This finding can be attributed to the fact that the inner legs make a large contribution to the hanging capacity at a small X_i/b and this contribution gradually lessens as X_i/b increases. Therefore, it is recommended that inner legs be used for beams with an X_i/b ratio equal to or less than 24% and diagonal bars be used for beams with X_i/b greater than 24%.

Punching shear

Estimates from code and specifications

Equations from the *PCI Design Handbook*, the ECP 207-2015, and the AASHTO LRFD specifications were used to estimate the punching shear capacities of the 10 ledge beams that were experimentally tested by Nafadi.⁸ The results of those calculations were then compared with the experimental results to investigate the conservativeness of the published equation.

Figure 23 shows that calculations for short-span ledge beams based on the AASHTO LRFD specifications were unconservative.

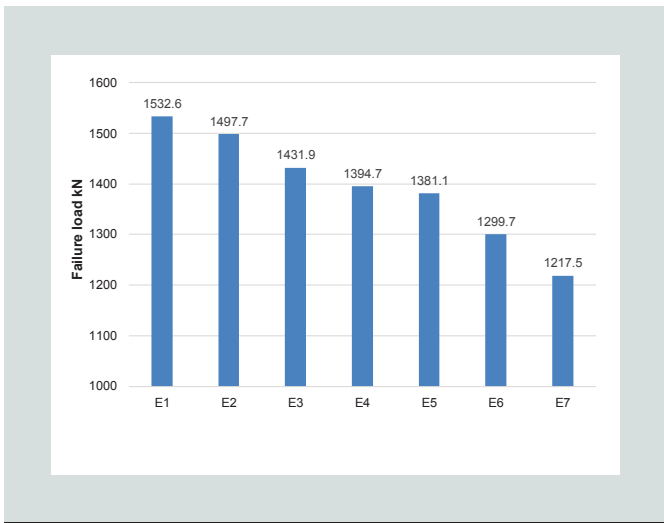


Figure 19. Load eccentricity effect. Note: 1 kN = 0.225 kip.

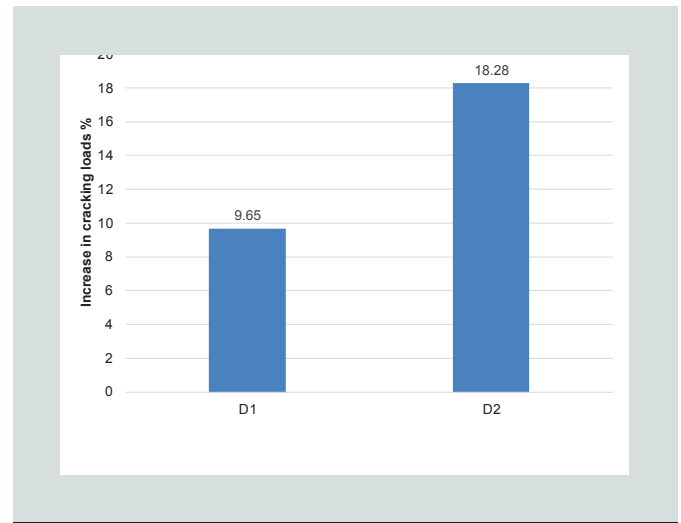


Figure 21. The increase in cracking loads of beams D1 and D2.

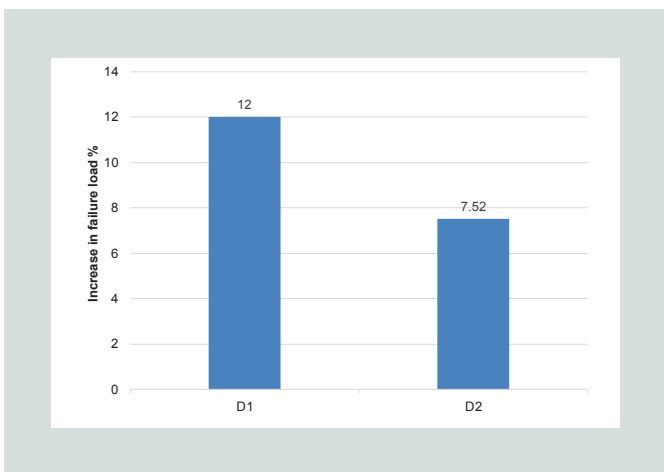


Figure 20. The increase in failure loads of beams D1 and D2.

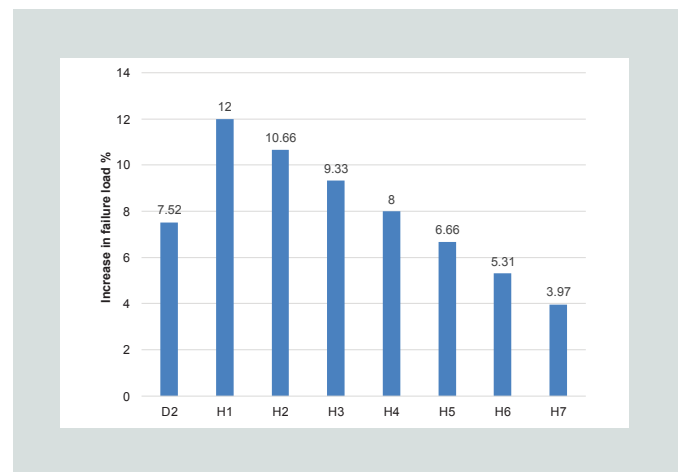


Figure 22. Diagonal bars compared with inner stirrups.

vative and overestimated the punching shear capacity of the ledges at midspan compared with the experimental results. On the other hand, calculations based on the *PCI Design Handbook* and ECP 207-2015 were conservative but underestimated the punching shear capacity at midspan compared with the experimental results.

Figure 24 shows that calculations for short-span ledge beams based on the AASHTO LRFD specifications were unconservative and overestimated the punching shear capacity of the ledges at ends compared with the experimental results. Calculations for the punching shear capacity at the ends of short-span ledge beams based on ECP 207-2015 were conservative for all but one test, and the *PCI Design Handbook* provided conservative and accurate estimates of the punching shear capacity at the short-span beam ends compared with the experimental results.

Figure 25 shows that calculations for long-span ledge beams

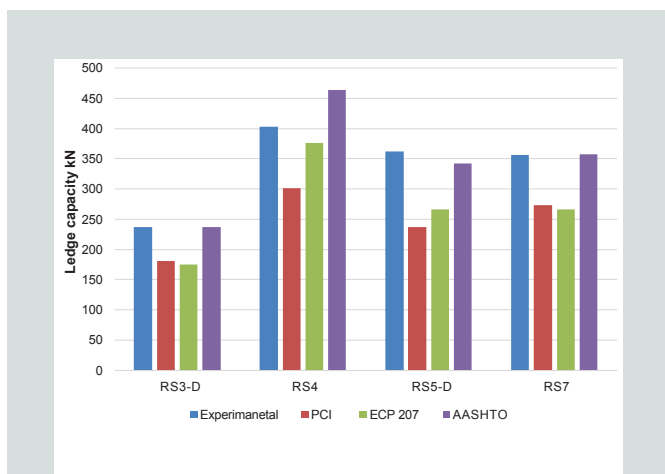


Figure 23. Load capacity at the midspans of short-span ledge beams comparison of experimental results and estimates derived from the *PCI Design Handbook*, ECP 207-2015, and AASHTO LRFD specifications. Note: 1 kN = 0.225 kip.

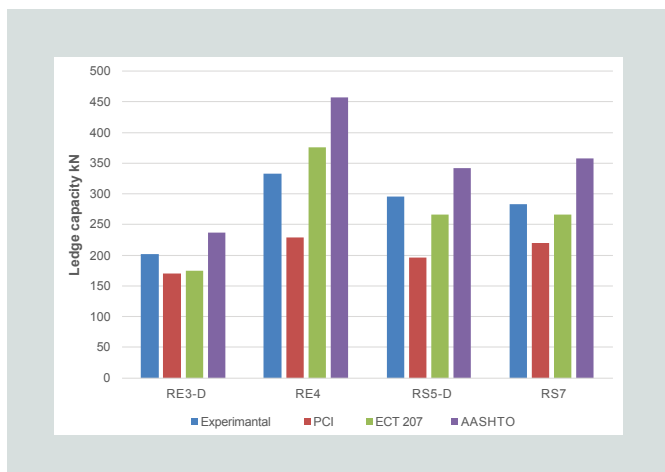


Figure 24. Load capacity at the ends of short-span ledge beams comparison of experimental results and estimates derived from the *PCI Design Handbook*, ECP 207-2015, and AASHTO LRFD specifications. Note: 1 kN = 0.225 kip.

based on the AASHTO LRFD specifications were unconservative and overestimated the punching shear capacity of the ledges at midspan compared with the experimental results, especially when they are exposed to high or moderate global stress. Calculations for the punching shear capacity at midspan of the long-span beams based on the *PCI Design Handbook* and the ECP 207-2015 were conservative compared with the experimental results. Results derived from the *PCI Design Handbook* underestimated the punching shear capacity at midspan, with the results being about half the experimental results. Therefore, the estimates derived from the *PCI Design Handbook* at midspan of long-span ledge beams can be considered conservative, but the equations need to be developed to give more accurate results. On the other hand, the ECP 207-2015 gave conservative and accurate estimates of the punching shear capacity at midspan.

Figure 26 shows that calculations for long-span ledge beams

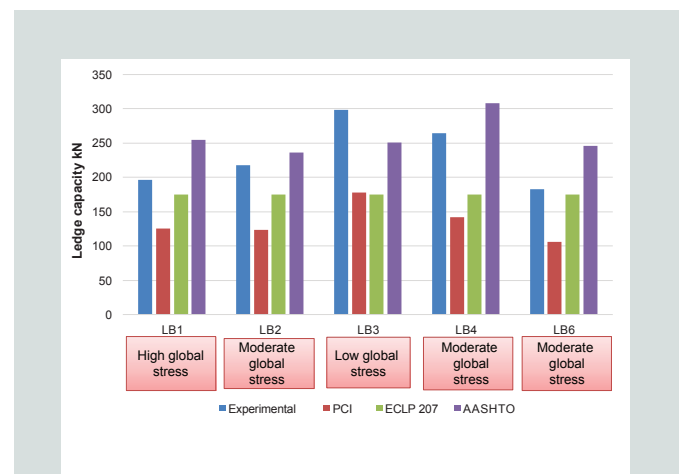


Figure 25. Load capacity at the midspans of long-span ledge beams comparison of experimental results and estimates derived from the *PCI Design Handbook*, ECP 207-2015, and AASHTO LRFD specifications. Note: 1 kN = 0.225 kip.

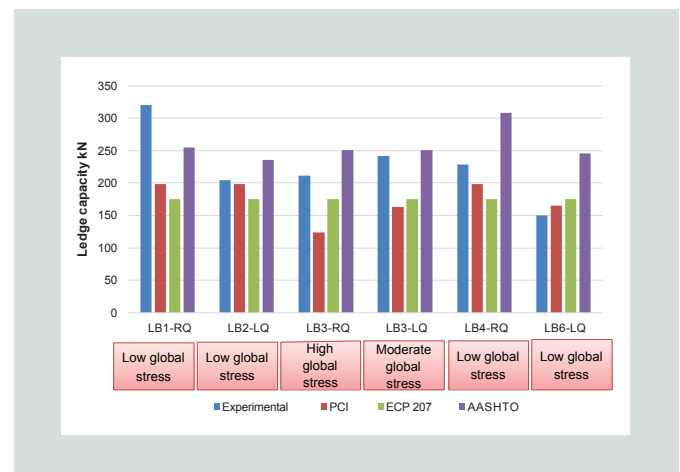


Figure 26. Load capacity at the quarter spans of long-span ledge beams comparison of experimental results and estimates derived from the *PCI Design Handbook*, ECP 207-2015, and AASHTO LRFD specifications. Note: 1 kN = 0.225 kip.

based on the AASHTO LRFD specifications were unconservative and overestimated the punching shear capacity of the ledges at quarter span compared with the experimental results. Results for the punching shear capacity at quarter span of long-span ledge beams based on the *PCI Design Handbook* and the ECP 207-2015 were conservative compared with the experimental results, except in one test. Because there was an outlier, the equations of the *PCI Design Handbook* and the ECP 207-2015 at quarter span of long-span ledge beams may need to be further investigated to confirm the otherwise conservative results.

Figure 27 shows that calculations for long-span ledge beams based on the AASHTO LRFD specifications and the ECP 207-2015 were unconservative and overestimated the punching shear capacity of the ledges at the ends compared with the experimental results. In contrast, calculations for the punching shear capacity at the ends of long-span ledge beams based

on the *PCI Design Handbook* were conservative compared with the experimental results for all tests. Therefore, the *PCI Design Handbook* methods for estimating punching shear capacity at the ends of long-span ledge beams can be considered conservative and accurate.

Finite element estimates

Nonlinear finite element software was used to model and analyze the 10 ledge beams that were experimentally tested by Nafadi.⁸ **Figures 28** through **32** compare the finite element estimates for the punching shear capacity of these beams with the experimental results. The results indicate good correlation between the finite element estimates and the experimental results.

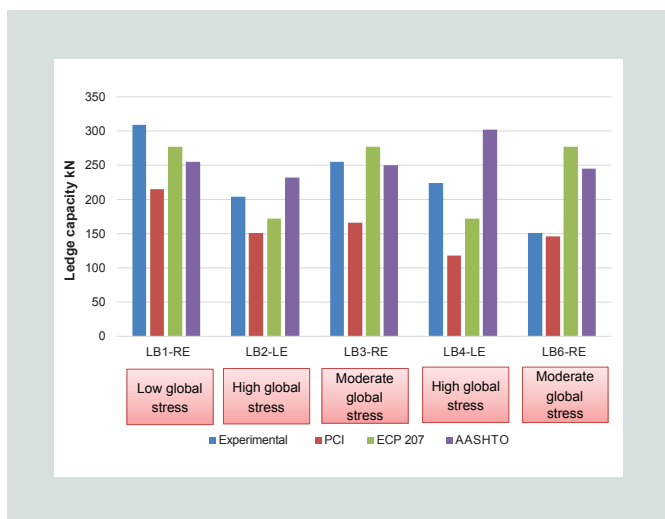


Figure 27. Load capacity at the ends of long-span ledge beams comparison of experimental results and estimates derived from the *PCI Design Handbook*, ECP 207-2015, and AASHTO LRFD specifications. Note: 1 kN = 0.225 kip.

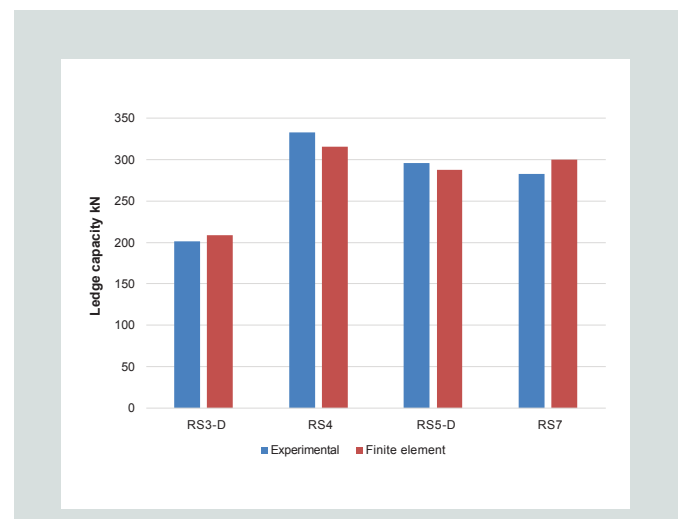


Figure 29. Ledge capacity of short-span ledge beams at ends comparison between the finite element model estimates and experimental results. Note: 1 kN = 0.225 kip.

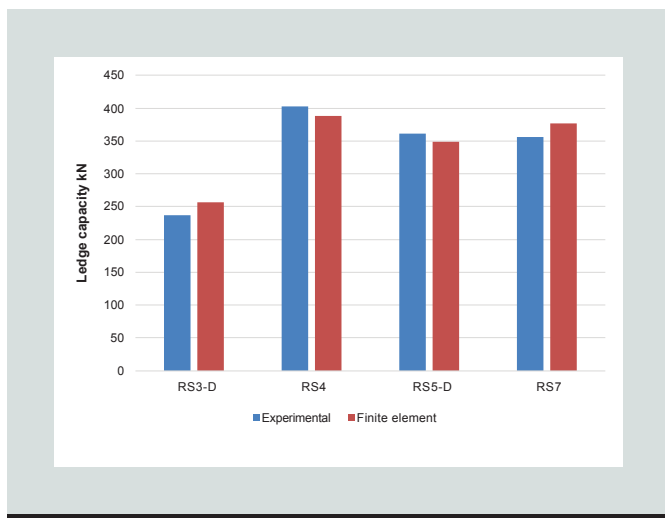


Figure 28. Ledge capacity of short-span ledge beams at mid-span comparison between the finite element model estimates and experimental results. Note: 1 kN = 0.225 kip.

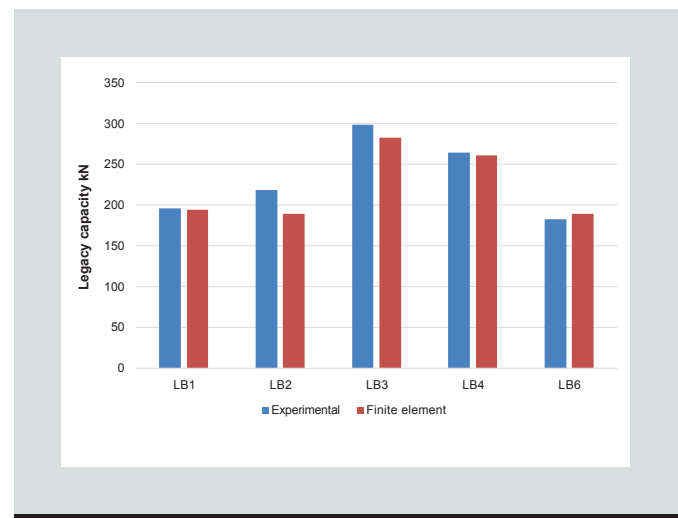


Figure 30. Ledge capacity of long-span ledge beams at mid-span comparison between the finite element model estimates and experimental results. Note: 1 kN = 0.225 kip.

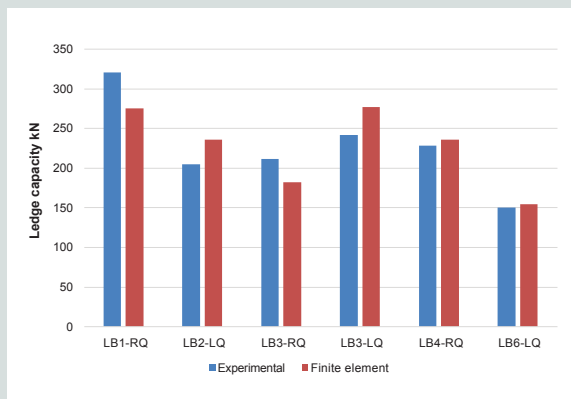


Figure 31. Ledge capacity of long-span ledge beams at quarter span comparison between the finite element model estimates and experimental results. Note: 1 kN = 0.225 kip.

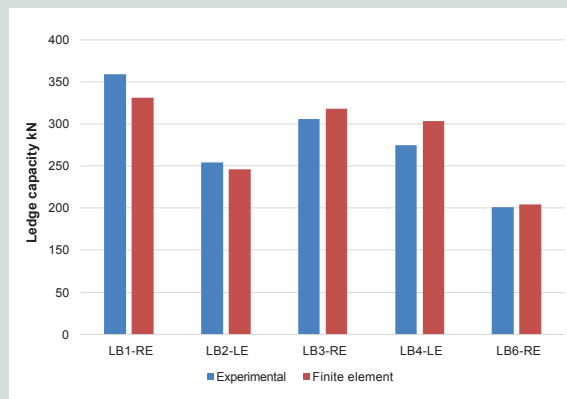


Figure 32. Ledge capacity of long-span ledge beams at ends comparison between the finite element model estimates and experimental results. Note: 1 kN = 0.225 kip.

Conclusion

This paper presents a theoretical investigation of the behavior of ledge beams by using the finite element theory to estimate the nonlinear behavior of reinforced concrete in all loading stages. Three main variables investigated in this study were the effective thickness of the outer part of the web near the concentrated load where vertical hangers can effectively be placed, the contribution of diagonal bars to the hanging capacity of ledge beams, and the effect of the load eccentricity on the hanging capacity of ledge beams. A plasticity-based nonlinear finite element model was used to analyze the punching behavior of ledge beams. Several experimental results were collected from the literature to support the results derived from the model. The study also compared provisions from selected codes and specifications to estimate the hanging capacity of ledge beams and the punching shear capacity of ledges. Last, the paper presents a proposal for the effective thickness of the outer part of the web near the concentrated load where vertical hangers can be effectively placed.

Based on the nonlinear finite element analysis performed in this research and the calculated estimates for the hanging capacity and the punching shear capacity of the investigated ledge beams, the following conclusions were drawn:

- The ECP 207-2015 and the AASHTO LRFD specifications overestimate the hanging capacity of ledge beams. The *PCI Design Handbook*, on the other hand, underestimates the hanging capacity because it does not consider the contribution of the inner stirrups' legs.
- Using the inner stirrups' legs as hanger reinforcement increased the hanging capacity of ledge beams depending on X_f/b . The hanging capacity is increased by decreasing the X_f/b . This finding is attributed to the fact that as the inner stirrups get closer to the outer one, their contribution to the hanging capacity becomes more noticeable. An inner stirrup located at X_f/b of about 20% could provide

an increase of about 10% to the hanging capacity.

- The load eccentricity has a pronounced effect on the hanging capacity of ledge beams. The hanging capacity of the analyzed beams decreased as the load eccentricity increased. For a load eccentricity of about 85% of the width of the ledge, the hanging capacity decreased by about 25% compared with the control beam.
- Calculations based on the ECP 207-2015 and the AASHTO LRFD specifications demonstrate that codes of practice that neglect the effect of the load eccentricity may overestimate the hanging capacity and their application could lead to unconservative design. The *PCI Design Handbook* accounts for the effect of the load eccentricity and results in conservative design. Therefore, it is recommended that codes and specifications include the load eccentricity effect in design equations.
- The use of diagonal bars increases both the cracking load and the failure load compared with the control beam. In this investigation, the use of diagonal bars increased the cracking and the failure loads by about 18.5% and 7.5%, respectively. The use of diagonal bars has a more pronounced effect on the cracking load.
- The hanging capacity of ledge beams can be increased either by using inner stirrups or diagonal bars. For the cases investigated in this study, the inner stirrups could be a more efficient choice when the X_f/b is less than about 25%.
- For the cases investigated in this study, there were good correlations between the nonlinear finite element estimates and the experimental results for the punching shear capacity of ledges.
- The equations proposed in the ECP 207-2015 to estimate the punching perimeter for interior and exterior loads, which are similar to those given in the AASHTO

LRFD specifications, should be revised and corrected to eliminate what could be a typing error.

- The ECP 207-2015 and the AASHTO LRFD specifications do not account for the interaction of flexure, one-way shear, and punching shear. They also do not take into consideration the effect of prestressing, if there is one. Those interactions are taken into consideration in the *PCI Design Handbook*. Moreover, the AASHTO LRFD specifications do not account for the effect of the load eccentricity on the punching shear capacity of ledges.
- The AASHTO LRFD specifications overestimated the punching shear capacity of the ledges of the short-span ledge beams compared with the experimental results. In contrast, results based on the *PCI Design Handbook* and the ECP 207-2015 were conservative.
- The AASHTO LRFD specifications overestimated the punching shear capacity of the ledges at midspan and quarter span of the long-span ledge beams compared with the experimental results. Estimates derived from *PCI Design Handbook* and the ECP 207-2015, on the other hand, were conservative.
- The AASHTO LRFD specifications and the ECP 207-2015 overestimated the punching shear capacity of the ledges at the ends of the long-span ledge beams compared with the experimental results, whereas estimates from the *PCI Design Handbook* were conservative.
- Among the investigated references and codes of practice, the *PCI Design Handbook* provided the most reliable estimates of hanging capacity, though those results may be overly conservative unless consideration is given to the inner leg of the stirrup. Moreover, the PCI estimates of punching shear capacities may be unduly conservative.

References

1. Fernandez-Gomez, E. 2012. "Design Criteria for Strength and Serviceability of Inverted-T Straddle Bent Caps." PhD diss., University of Texas, Austin. <https://hdl.handle.net/2152/ETD-UT-2012-08-6340>.
2. Larson, N. A. 2013. "Design of Reinforced Concrete Inverted-T Beams for Strength and Serviceability." PhD diss., University of Texas, Austin. <https://hdl.handle.net/2152/21270>.
3. Garber, D. B., N. Larson Varney, E. Fernández Gomez, and O. Bayrak. 2017. "Performance of Ledges in Inverted-T Beams." *ACI Structural Journal* 114 (2):487–498. <https://doi.org/10.14359/51689451>.
4. AASHTO (American Association of State Highway and Transportation Officials). 2020. *AASHTO LRFD Bridge Design Specifications*. 9th ed. Washington, DC: AASHTO.
5. Kamara, M., and L. Novak. 2017. *PCA Notes on ACI 318-11 Building Code Requirements for Structural Concrete with Design Applications*. Skokie, IL: Portland Cement Association.
6. HBRC (Housing and Building National Research Center), Ministry of Housing and Urban Communities. 2015. *The Egyptian Code of Practice for Planning, Design, and Construction of Bridges and Elevated Intersections*. ECP 207-2015. Giza, Egypt: HBRC.
7. PCI. 2017. *PCI Design Handbook: Precast and Prestressed Concrete*. 8th ed. MNL 120-17. Chicago, IL: PCI. <https://doi.org/10.15554/MNL-120-17>.
8. Nafadi, M. K. M. 2016. "Behavior and Design of Ledges of L-Shaped Beams." PhD diss., North Carolina State University. <http://www.lib.ncsu.edu/resolver/1840.20/33275>.
9. Nafadi, M. K., O. M. Khalafalla, G. W. Lucier, S. Rizkalla, P. Zia, and G. J. Klein. 2018. "Ledge Behavior and Strength of Short-Span L-Shaped Beams." *PCI Journal* 63 (2): 67–86. <https://doi.org/10.15554/pcij63.2-04>.
10. Nafadi, M. K., G. W. Lucier, S. Rizkalla, P. Zia, and G. J. Klein. 2018. "Ledge Behavior and Strength of Long-Span L-Shaped Beams." *PCI Journal* 63 (2): 50–66. <https://doi.org/10.15554/pcij63.2-01>.
11. Nafadi, M. K., G. W. Lucier, S. Rizkalla, P. Zia, and G. J. Klein. 2018. "Development of Design Guidelines for Ledges of L-Shaped Beams." *PCI Journal* 63 (2): 32–45. <https://doi.org/10.15554/pcij63.2-05>.
12. Lubliner, J., J. Oliver, S. Oller, and E. Oñate. 1989. "A Plastic Damage Model for Concrete." *International Journal of Solids and Structures* 25 (3): 299–326. [https://doi.org/10.1016/0020-7683\(89\)90050-4](https://doi.org/10.1016/0020-7683(89)90050-4).
13. Kmiecik, P., and M. Kamiński. 2011. "Modelling of Reinforced Concrete Structures and Composite Structures with Concrete Strength Degradation Taken into Consideration." *Archives of Civil and Mechanical Engineering* 11 (3): 623–636. [https://doi.org/10.1016/S1644-9665\(12\)60105-8](https://doi.org/10.1016/S1644-9665(12)60105-8).
14. European Committee for Standardization. 2004. *Eurocode 2: Design of Concrete Structures – Part 1-1: General Rules and Rules for Buildings*. Brussels, Belgium: European Commission.
15. Genikomsou, A. S., and M. A. Polak. 2015. "Finite Element Analysis of Punching Shear of Concrete Slabs Using Damaged Plasticity Model in Abaqus." *Engineering Structures* 98: 38–48. <https://doi.org/10.1016/j.engstruct.2015.04.016>.

16. Alwathaf, A. H., A. Ali, M. S. Jaafar, and M. A. Algorafi. 2011. "Stress-Strain Modelling of Reinforced Concrete Membrane Structures." *International Journal of Physical Sciences* 6 (30): 6820–6828. <https://doi.org/10.5897/IJPS11.468>.

17. Nayal, R., and H. A. Rasheed. 2006. "Tension Stiffening Model for Concrete Beams Reinforced with Steel and FRP Bars." *Journal of Materials in Civil Engineering* 18 (6): 831–841. [https://doi.org/10.1061/\(ASCE\)0899-1561\(2006\)18:6\(831\)](https://doi.org/10.1061/(ASCE)0899-1561(2006)18:6(831)).

18. Wang, T., and T. T. C. Hsu. 2001. "Nonlinear Finite Element Analysis of Reinforced Concrete Structures Using New Constitutive Models." *Computers and Structures* 79 (32): 2781–2791. [https://doi.org/10.1016/S0045-7949\(01\)00157-2](https://doi.org/10.1016/S0045-7949(01)00157-2).

19. Carriera, D. J., and K. H. Chu. 1986. "Stress-Strain Relationship for Reinforced Concrete in Tension." *ACI Journal* 83 (1): 21–28. <https://doi.org/10.14359/1756>.

20. Lim, W. T. 1991. "Statistical Analysis of Reinforcing Steel Properties." MSc thesis, University of Canterbury. <https://doi.org/10.26021/3107>.

21. El Badawy, Y. 2012. "Contribution of Inner Stirrups with the Hanger Steel Reinforcement on the Behaviour of Ledge Beam." PhD diss., Ain Shams University, Abbasseya, Egypt.

22. Zhu, R. R. H., H. Dhonde, and T. T. C. Hsu. 2003. "Crack Control for Ledges in Inverted 'T' Bent Caps." Dept. of Civil & Environmental Engineering, The University of Houston. Technical report 2003, 0-1854-5. Texas Department of Transportation Research Report 0-1854-5. <https://static.tti.tamu.edu/tti.tamu.edu/documents/0-1854-5.pdf>.

23. ACI (American Concrete Institute) Committee 224. 2008. *Control of Cracking in Concrete Structures* (Reapproved 2008). ACI PRC-224R-01. Farmington Hills, MI: ACI.

24. Hassan, T. K. 2007. "Finite Element Study of Shear Behavior of Spandrel Ledges and Comparison with PCI Shear Design Provisions." *Advances in Structural Engineering* 10 (5): 475–485. <https://doi.org/10.1260/136943307782417690>.

c	= concrete cover
C	= distance between the center line of the exterior load and the edge of the ledge
d	= damage parameter
d_b	= diameter of the bottom reinforcing bars in the ledge
d_e	= effective depth of the ledge (distance from the bottom of the ledge to the center of the top flexural reinforcing bars in the ledge)
D	= abbreviation for deviatoric plan
e	= load eccentricity
E_c	= modulus of elasticity of concrete
E_o	= initial undamaged elastic modulus of concrete
E_s	= modulus of elasticity of steel
E_{sec}	= secant modulus of elasticity
E_{sh}	= modulus of elasticity of steel at strain hardening or the plastic modulus of elasticity of steel
E_t	= modulus of elasticity of concrete in tension
f_c	= uniaxial compressive stress
f'_c	= compressive strength of concrete
f_{cc}	= biaxial compressive stress
f_i	= tension stress
f_m	= mean stress
f_{su}	= ultimate tensile strength of steel reinforcing bars
f_t	= tensile stress
f_u	= ultimate stress of steel
f_y	= yield stress of steel
F	= strain in the ledge flexural reinforcement
G	= flow potential function
H	= strain in the hanger reinforcement
K_c	= ratio between the distances of the tension meridian and the compression meridian on the hydrostatic axis

Notation

a_f	= distance between the load center line and the hanger reinforcement
A_{sh}	= area of one of the reinforcing bars used as hanger reinforcement
b	= width of the web

L_E	= distance from the beam end and the center of the first exterior load	ε_{pl}	= plastic strain of concrete
L_{HF}	= compatibility-aided strut-and-tie model gauge length	ε_c^{pl}	= plastic compressive strain in concrete
n	= rate of weakening	ε_t^{pl}	= plastic tensile strain in concrete
p	= proposed beam under consideration	ε_{sh}	= strain in steel reinforcement at the strain hardening stage
\bar{p}	= effective hydrostatic pressure	ε_{su}	= strain in steel reinforcement corresponding to the peak strength
P	= axial load	ε_t	= tension strain
P_w	= yield surface in the deviatoric plan	ε_u	= ultimate strain
P_z	= failure surface in the deviatoric plan	Θ	= lode angle
\bar{q}	= equivalent von Mises stress	σ	= abbreviation for stress
S	= scaling ratio	$\bar{\sigma}$	= effective stress
S_1	= major principal effective stress	σ_1	= major effective principal stress
S_2	= intermediate principal effective stress	σ_2	= intermediate effective principal stress
S_3	= minor principal effective stress	σ_3	= minor effective principal stress
T	= tested beam	σ_{bo}	= biaxial compressive strength
ν_c	= Poisson's ratio for concrete	σ_c	= concrete stress
W	= crack width at the web-to-ledge junction	$\bar{\sigma}_c$	= effective compressive stress
X_i	= inner stirrup leg distance from the outer face of the web	σ_{co}	= uniaxial compressive strength
α	= dimensionless material constant	σ_m	= hydrostatic stress
β	= dimensionless material constant	$\bar{\sigma}_{max}$	= algebraically maximum eigenvalues of tensor
γ	= dimensionless material constant	σ_t	= tension stress
ε	= total strain	σ_{to}	= uniaxial tensile strength
ε_c	= concrete strain	τ_{oct}	= octahedral shear stress
ε_{cr}	= cracking strain	ϕ	= dilation angle that physically represents the internal friction angle of concrete
ε_F	= strain in the ledge flexural reinforcement	ε	= eccentricity that is a positive value expressing the rate of approach of the plastic potential hyperbola to its asymptote
ε_H	= strain in the hanger reinforcement		
ε_{HF}	= crack width strain		
ε_o	= strain corresponding to the peak stress		

About the author



Ahmed S. Alsharkawy is a master student at the Department of Structural Engineering at the faculty of engineering at Cairo University in Egypt.

Abstract

This paper presents a theoretical investigation of the behavior of reinforced concrete ledge beams that used finite element theory to model the nonlinear behavior of reinforced concrete in all loading stages. The three main parameters were the effective thickness of the outer part of the web near the concentrated load where vertical hangers can effectively be placed; the contribution of diagonal bars to the hanging capacity of ledge beams; and the effect of the load eccentricity on the hanging capacity of ledge beams. The punching shear behavior of ledge beams was also analyzed using a plasticity-based nonlinear finite element model. Several experimental results were collected from the literature to support the finite element results. The paper also compares estimates of the hanging capacity of ledge beams and the punching shear capacity of ledges derived from the *Egyptian Code of Practice for Planning, Design, and Construction of Bridges and Elevated Intersections*, the American Association of State Highway and Transportation Officials' *AASHTO LRFD Bridge Design Specifications*, and the *PCI Design Handbook: Precast and Prestressed Concrete*. Last, the paper presents a proposal for the effective thickness of the outer part of the web near the concentrated load where vertical hangers can be effectively placed.

Keywords

Hanger reinforcement, ledge beams, nonlinear finite element analysis, punching shear, reinforced concrete.

Review policy

This paper was reviewed in accordance with the Precast/Prestressed Concrete Institute's peer-review process. The Precast/Prestressed Concrete Institute is not responsible for statements made by authors of papers in *PCI Journal*. No payment is offered.

Publishing details

This paper appears in *PCI Journal* (ISSN 0887-9672) V. 70, No. 3, May-June 2025, and can be found at <https://doi.org/10.15554/pcij70.3-03>. *PCI Journal* is published bimonthly by the Precast/Prestressed Concrete Institute, 8770 W. Bryn Mawr Ave., Suite 1150, Chicago, IL 60631. Copyright © 2025, Precast/Prestressed Concrete Institute.

Reader comments

Please address any reader comments to *PCI Journal* editor-in-chief Tom Klemens at tklemens@pci.org or Precast/Prestressed Concrete Institute, c/o *PCI Journal*, 8770 W. Bryn Mawr Ave., Suite 1150, Chicago, IL 60631. 